Monthly Notices
of the
ROYAL ASTRONOMICAL SOCIETY

MNRAS **496,** L33–L37 (2020)
Advance Access publication 2020 May 15

doi:10.1093/mnrasl/slaa085

Correlations between mass, stellar kinematics, and gas metallicity in EAGLE galaxies

L. J. Zenocratti,[1,2] M. E. De Rossi,[3,4]★ M. A. Lara-López [5] and T. Theuns[6]

[1] *Facultad de Ciencias Astronómicas y Geofísicas, Universidad Nacional de La Plata, Paseo del Bosque s/n, B1900FWA La Plata, Argentina*
[2] *Instituto de Astrofísica de La Plata (IALP), UNLP - CONICET, Paseo del Bosque s/n, B1900FWA La Plata, Argentina.*
[3] *Universidad de Buenos Aires, Facultad de Ciencias Exactas y Naturales y Ciclo Básico Común. CC 67, Suc. 28, 1428, Buenos Aires, Argentina*
[4] *CONICET-Universidad de Buenos Aires, Instituto de Astronomía y Física del Espacio (IAFE). CC 67, Suc. 28, 1428, Buenos Aires, Argentina*
[5] *DARK, Niels Bohr Institute, University of Copenhagen, Lyngbyvej 2, DK-2100 Copenhagen, Denmark*
[6] *Institute for Computational Cosmology, Department of Physics, Durham University, South Road, Durham DH1 3LE, UK*

Accepted 2020 May 5. Received 2020 April 14; in original form 2019 November 20

ABSTRACT

The metallicity of star-forming gas in galaxies from the EAGLE (Evolution and Assembly of GaLaxies and their Environments) simulations increases with stellar mass. Here, we investigate whether the scatter around this relation correlates with morphology and/or stellar kinematics. At redshift $z = 0$, galaxies with more rotational support have lower metallicities on average when the stellar mass is below $M_\star \approx 10^{10}$ M$_\odot$. This trend inverts at higher values of $M_\star$, when prolate galaxies show typically lower metallicity. At increasing redshifts, the trend between rotational support and metallicity becomes weaker at low stellar mass but more pronounced at high stellar mass. We argue that the secondary dependence of metallicity on stellar kinematics is another manifestation of the observed anticorrelation between metallicity and star formation rate at a given stellar mass. At low masses, such trends seem to be driven by the different star formation histories of galaxies and stellar feedback. At high masses, feedback from active galactic nuclei and galaxy mergers plays a dominant role.

Key words: galaxies: abundances - galaxies: evolution - galaxies: high-redshift - galaxies: star formation - cosmology: theory.

1 INTRODUCTION

The relation between stellar mass and gas-phase metallicity in galaxies (henceforth the mass–metallicity relation, MZR) has been studied extensively in the last decades from both an observational (Tremonti et al. 2004; Lara-López et al. 2010) and a theoretical (Calura et al. 2009; Yates, Kauffmann & Guo 2012; De Rossi et al. 2015, 2017, hereafter, DR17; Sharma & Theuns 2019) point of view. At redshift $z \sim 0$, gas metallicity, Z, increases with stellar mass, $M_\star$, approximately as a power law, $Z \propto M_\star^{2/5}$; the slope of the correlation flattens towards higher masses. This power-law trend is also seen at higher redshifts, though possibly with a different slope and normalization (e.g. Troncoso et al. 2014).

The scatter along the observed MZR correlates with other properties of galaxies. Ellison et al. (2008) showed that, at a given stellar mass, observed galaxies with smaller half-mass radii or lower specific star formation rates (sSFRs) tend to have higher gas metallicity, as quantified by the oxygen abundance, O/H. To account for these observations, Lara-López et al. (2010) and Mannucci et al. (2010) suggested the existence of a three-dimensional relation between $M_\star$, O/H, and SFR, where systems with higher SFRs tend to have lower O/H at a given value of $M_\star$. Alternatively, this three-dimensional relation could result from a more fundamental underlying relation between $M_\star$, O/H, and *gas fraction* (f_g), since f_g and SFR correlate (e.g. Bothwell et al. 2013; Lara-López et al. 2013). Deciding which relation is more fundamental could be helped by examining other correlations. Recent observations suggest that Z tends to be lower in galaxies with a higher concentration, higher Sérsic index, or higher SFR (Wu, Zhang & Zhao 2019), at given value of $M_\star$. Unfortunately, surprisingly large uncertainties remain in inferring physical relations from the data because different methods yield significantly different answers (e.g. Telford et al. 2016). In fact, some observational studies do not find that the scatter around the MZR correlates with SFR (e.g. Sánchez et al. 2019), and some studies claim that the correlation exists, but inverts at high $M_\star$ (e.g. Yates et al. 2012).

In this paper, we examine the scatter around the MZR in galaxies from the EAGLE (Evolution and Assembly of GaLaxies and their Environments) cosmological hydrodynamical simulations (Schaye et al. 2015). The EAGLE suite of cosmological hydrodynamical simulations uses subgrid models calibrated to reproduce a small set of observations at $z \approx 0$, as described in Crain et al. (2015).

★ E-mail: mariaemilia.dr@gmail.com

The simulations then reproduce a relatively extensive set of other observations, including the evolution of the galaxy stellar mass function (Furlong et al. 2015), of galaxy sizes (Furlong et al. 2017), of optical (Trayford et al. 2015), and ultraviolet and infrared luminosities (Camps et al. 2018). DR17 analysed the secondary metallicity dependences in EAGLE (including the dependences on SFR, sSFR, f_g, and stellar age, $t_\star$), obtaining good agreement with observed trends (see also Lara-López et al. 2019). In particular, DR17 show that EAGLE galaxies follow remarkably well the observed 'fundamental metallicity relation' introduced by Mannucci et al. (2010). In addition, Sánchez Almeida & Dalla Vecchia (2018) show that EAGLE simulations are able to reproduce the observed secondary metallicity dependence on the size of galaxies.

In this letter, we report new predictions of EAGLE simulations regarding the connection between MZR scatter and internal morpho-kinematics of galaxies. Such trends were not previously reported in MZR studies. In a forthcoming article, we address the origin of these metallicity secondary dependences by analysing the formation histories of different galaxy populations. This letter is organized as follows. In Section 2, we briefly describe the EAGLE simulations and the galaxy selection criteria. In Section 3, we analyse the simulated MZR as a function of the morphology and kinematics of the galaxies. We discuss the origin of our obtained trends in Section 4. We summarize our findings in Section 5.

2 THE EAGLE SIMULATIONS

A full description of the EAGLE simulation suite is given by Schaye et al. (2015). Briefly, the suite was simulated with the GADGET-3 incarnation of the TREEPM-SPH code described by Springel (2005), with subgrid modules for physics whose parameters are calibrated to reproduce the $z \approx 0$ galaxy stellar mass function, the relation between galaxy mass and size, and the black hole (BH) mass–stellar mass relation (Crain et al. 2015). The adopted cosmological parameters are taken from Planck Collaboration XXIII (2015): $\Omega_\Lambda = 0.693$, $\Omega_m = 0.307$, $\Omega_b = 0.04825$, $n_s = 0.9611$, $Y = 0.248$, and $h = 0.677$.

EAGLE consists of simulations with various box sizes and particle masses. Here, we mainly use simulation labelled 'Ref-L100N1504' in Schaye et al. (2015), which has a comoving extent of $L = 100$ comoving megaparsecs (cMpc) and a baryonic particle mass of $\sim 1.2 \times 10^6$ M$_\odot$ (corresponding to 1504^3 particles). We have verified that the main trends and conclusions presented in this work are consistent with those from the higher resolution EAGLE simulation 'Recal-L025N0752', analysed previously by DR17.

EAGLE galaxies are identified using a combination of the 'friends-of-friends' (FOF) and SUBFIND algorithms. This picks out 'self-bound' structures of gas, stars, and dark matter. Here, we analyse the properties of both central galaxies (the dominant galaxies in FOF haloes) and satellites.[1] Following DR17, we measure baryonic properties within spherical apertures of 30 proper kiloparsecs (pkpc) and characterize the 'metallicity' of star-forming gas by its O/H abundance (EAGLE tracks 11 abundances, including oxygen and hydrogen). We analyse galaxies with at least 25 star-forming gas particles (gas mass at least 5.25×10^7 M$_\odot$), which we found to be a reasonable compromise between numerical resolution and bias. To characterize the stellar morphology and kinematics, we use the fraction of kinetic energy in corotation, κ_{co}, the disc-to-total stellar mass ratio, D/T, the ratio V/σ of stellar rotation to velocity dispersion, the ellipticity, $\epsilon_\star$, of the stellar body, and its triaxiality, T. These were computed by Thob et al. (2019) and can be queried in the EAGLE database[2] (McAlpine et al. 2016; The EAGLE Team 2017).

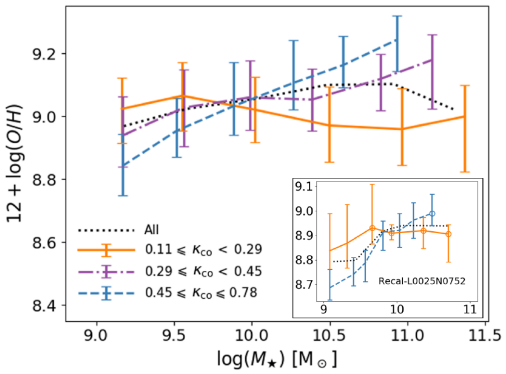

Figure 1. Black dotted line: median $M_\star$–O/H (MZR) relation in redshift $z = 0$ EAGLE galaxies from simulation Ref-L100N1504. Coloured lines: MZR relation for EAGLE galaxies binned by κ_{co}, the fraction of stellar kinetic energy in rotation: the lowest third κ_{co} (orange), intermediate κ_{co} (purple), and the highest third κ_{co} (blue). Error bars encompass the 25th and 75th percentiles. Inset: as main panel, but for the higher resolution EAGLE simulation Recal-L0025N0752.

3 CORRELATING MORPHOLOGY AND METALLICITY

EAGLE's $z = 0$ MZR is plotted in Fig. 1, with galaxies binned by κ_{co}, the fraction of stellar kinetic energy of the galaxy that is invested in ordered rotation. Below $M_\star \sim 10^{10}$ M$_\odot$, dispersion-supported galaxies (low κ_{co}, orange line) have higher O/H than rotationally supported galaxies (blue line) of the same $M_\star$. Also striking is that O/H increases with $M_\star$ for rotationally supported galaxies, but is almost independent of $M_\star$ for dispersion-supported galaxies. As a consequence, the trend between O/H and κ_{co} inverts above $M_\star \approx 10^{10}$ M$_\odot$, with massive dispersion-supported galaxies having *lower* O/H than rotationally supported galaxies of the same mass. We find similar trends in the higher resolution simulation Recal-L025N0752 (inset of Fig. 1).

The results of Fig. 1, combined with the dependence of O/H on the SFR, sSFR, and the gas fraction reported by DR17, suggest that κ_{co} may itself correlate with these other galaxy parameters. We examine this in Fig. 2. Independent of $M_\star$, the gas fraction (middle panel) and the sSFR (right-hand panel) both increase with κ_{co}, the increase of f_g being the most pronounced for the lower $M_\star$ galaxies (blue line), whereas the increase of the sSFR is more evident in the higher $M_\star$ galaxies (purple line). The sSFR is a measure of the rate at which metals are produced and f_g is a measure of the size of the reservoir that dilutes those metals. Therefore, a consequence of these trends is that O/H *decreases* with increasing κ_{co} at low $M_\star$, whereas it *increases* for high-mass galaxies (see the left-hand panel); at $M_\star \sim 10^{10}$ M$_\odot$, O/H does not depend on κ_{co}. These findings are consistent with the relation between colour and kinematics of EAGLE galaxies studied by Correa et al. (2017). Our results are also consistent with the observations by Calvi et al. (2018) that late-type galaxies have higher SFR and sSFR compared to S0 and elliptical galaxies of the same mass.

[1] Our main results are unchanged if we analyse only centrals.

[2] http://eagle.strw.leidenuniv.nl, http://www.eaglesim.org/

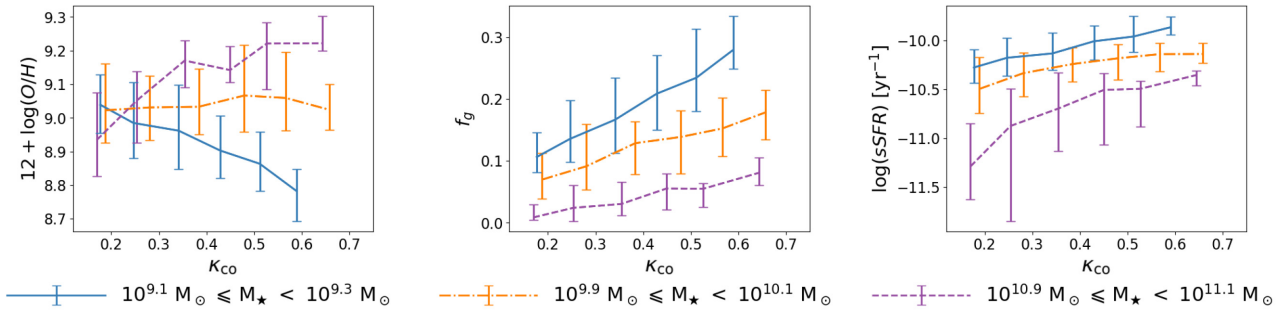

Figure 2. Correlation between O/H (left-hand panel), gas fraction f_g (middle panel), and the sSFR (right-hand panel) and κ_{co}, the fraction of stellar kinetic energy in rotation, for $z = 0$ EAGLE galaxies from simulation Ref-L100N1504. Galaxies are binned in stellar mass: low stellar mass (blue), intermediate stellar mass (orange), and high stellar mass (purple); see legend. Curves represent the median relation; error bars encompass the 25th and 75th percentiles.

How these correlations arise is analysed in more detail[3] in Fig. 3. At $M_\star < 10^{10}$ M$_\odot$, galaxies typically have low κ_{co}, but there is a tail of galaxies with high κ_{co} and low O/H: this tail generates the anticorrelation between κ_{co} and O/H in Fig. 2. These outliers are also gas-rich and have unusually high stellar ellipticities, $\epsilon_\star$, and low triaxiality parameter T. At $M_\star > 10^{10}$ M$_\odot$, galaxies have usually a high value of κ_{co}, but now there is a tail of galaxies with low κ_{co} and high T that are typically more massive and have low O/H. At intermediate masses, $M_\star \sim 10^{10}$ M$_\odot$, there is relatively little variation in κ_{co} or $\epsilon_\star$.

We plot the MZR relation at different redshifts z in the left-hand panel of Fig. 4. At a given z, the sample of simulated galaxies is separated in two subsamples, using the median value of κ_{co} ($\bar{\kappa}_{co}$) at that z. Note that the value of $\bar{\kappa}_{co}$ tends to decrease with increasing z: dispersion-supported galaxies increasingly dominate at higher z. As expected, the normalization of the MZR decreases with z, with such evolution being independent of κ_{co} at $M_\star \sim 10^{10}$ M$_\odot$. As we also noticed at $z = 0$, there is a clear increase of O/H with $M_\star$ for galaxies with high κ_{co}, but this trend is mostly absent for the low-κ_{co} galaxies. At the low-mass end ($M_\star \lesssim 10^{10}$ M$_\odot$), the secondary dependence of O/H on κ_{co} tends to vanish as z increases, due mainly to an increase of the MZR slope for systems with $\kappa_{co} < \bar{\kappa}_{co}$ at $z \gtrsim 1$. On the other hand, at high masses ($M_\star \gtrsim 10^{10}$ M$_\odot$), the secondary dependence of O/H on κ_{co} tends to be stronger at higher z, which, in this case, is caused by an increase of the MZR slope for systems with $\kappa_{co} > \bar{\kappa}_{co}$ at $z \gtrsim 2$. Similar evolutionary trends are obtained when using other morpho-kinematical indicators.

4 DISCUSSION

Reproducing observed metallicity scaling relations is an important test of current cosmological hydrodynamical simulations, with many of them showing good agreement with observations (e.g. DR17; Davé et al. 2019; Torrey et al. 2019). In this context, metal-poor gas inflows have been suggested to play a key role in driving secondary O/H dependences (at a given mass) on galaxy sizes (e.g. Sánchez Almeida & Dalla Vecchia 2018), SFRs, and gas fractions (e.g. DR17).

In addition, Torrey et al. (2018) claimed that similar evolution time-scales of SFR and O/H may be required to explain the O/H–$M_\star$–SFR relation in the *Illustris-TNG* simulations. For more massive galaxies, mergers and active galactic nuclei (AGNs) might also play a crucial role in shaping the MZR (e.g. DR17; Ma et al. 2016). Although different works have focused on the O/H dependence on SFR, its relation with morpho-kinematics has not been discussed before. As a consistency check, we analysed the dependence of MZR on morpho-kinematics in the *Illustris-TNG* simulations, obtaining similar general trends to those shown in Fig. 1: at low masses, galaxies with higher D/T ratios generally have lower O/H, and the opposite is true for more massive systems. Hence, generally, such trends seem to be robust against the details of physical implementations adopted in these models. Nevertheless, we highlight that the detailed features of metallicity scaling relations (e.g. detailed shape, scatter, and normalization) do depend on the different model prescriptions; this work is focused on predictions from the EAGLE model.

Calura et al. (2009) analysed the MZR of galaxies using 'chemical evolution' models. They did not find a clear dependence of O/H on morphology at a given mass and z, which might be a consequence of the different assumptions made in their models. For example, they assume that galaxies retain the same morphology throughout their evolution and they neglect mergers. In contrast, in the EAGLE simulations, discs may be destroyed during mergers and may regrow following accretion (Trayford et al. 2019).

In the middle panel of Fig. 4, we show the EAGLE $z = 0$ MZR binned according to the cosmic time, $t_{\star,50}$, when galaxies reached half of their present stellar mass, $M_\star$. At the low-mass end, systems with lower O/H tend to have been formed at later times. These systems also show higher sSFRs, higher gas fractions, and lower stellar ages (DR17), exhibiting also higher rotational support and disky morphologies (Figs 1 and 3). An analysis of the formation histories of these galaxies suggests that such trends would be associated with the accumulated effects of accretion of metal-poor gas at *late* times (generally, $z \lesssim 1$), which dilutes the metal content of galaxies, triggers their star formation activity, and contributes to the formation of the galaxy disc.[4] This is consistent with the left-hand panel of Fig. 4, which shows that the dependence of the low-mass MZR on κ_{co} is more significant towards $z = 0$.

The right-hand panel of Fig. 4 shows the MZR binned according to the BH–stellar mass ratio ($M_{BH}/M_\star$). Massive galaxies with higher $M_{BH}/M_\star$ tend to have lower O/H. This is consistent with the results of DR17, who claimed that AGNs quench the metallicity evolution of galaxies by heating the gas, suppressing the star formation activity, and ejecting metals out of the systems. Thus, at the high-mass end, less metal-enriched systems have lower sSFRs, lower fraction of

[3]Similar results are obtained if using D/T or V/σ instead of κ_{co}.

[4]Long-term gas accretion could occur continuously or by successive gas inflow events.

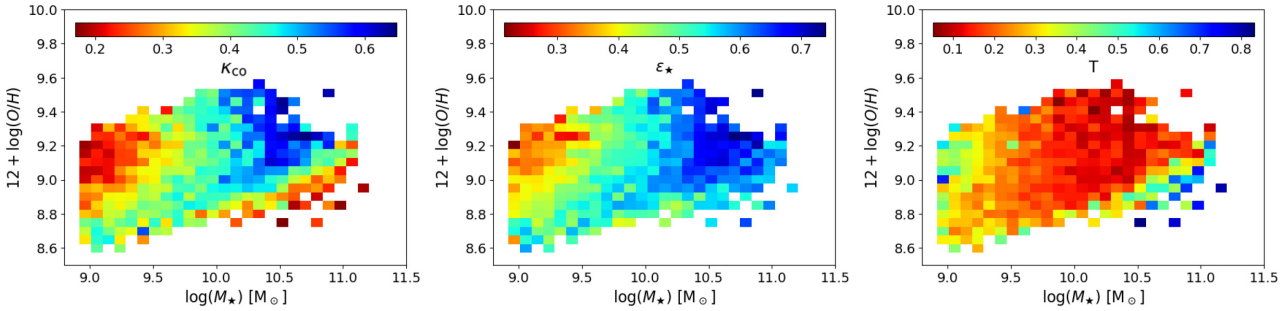

Figure 3. O/H metallicity as a function of stellar mass, $M_\star$, for $z = 0$ EAGLE galaxies from simulation Ref-L100N1504. Bins in O/H–$M_\star$ are coloured according to the median value of $\kappa_{\rm co}$ (left-hand panel), the stellar ellipticity $\epsilon_\star$ (middle panel), and the galaxy's triaxiality parameter T (right-hand panel).

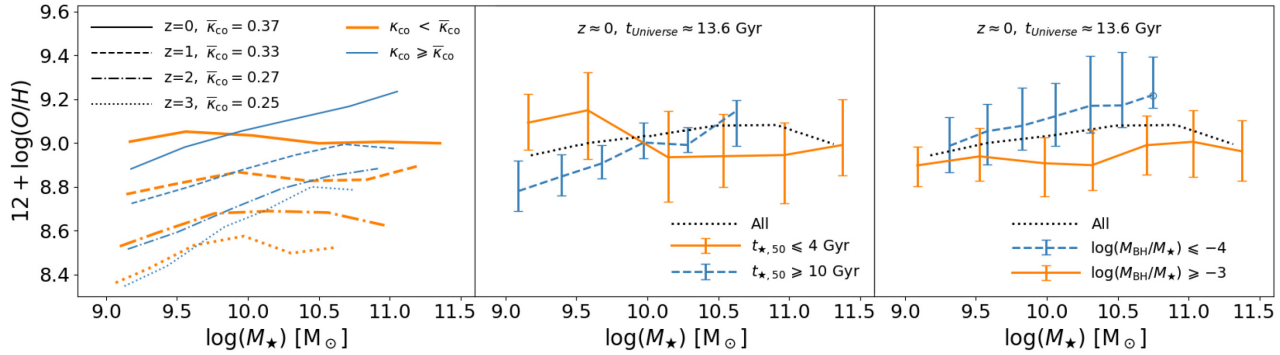

Figure 4. Left-hand panel: MZR at different z, as indicated in the figure. Curves representing galaxies with rotational support below the median at the given z are plotted in thick orange, and those with higher $\kappa_{\rm co}$ are plotted in thin blue. Middle and right-hand panels: $z = 0$ MZRs binned according to $t_{\star,50}$ (the time when galaxies reached half of their present $M_\star$) and $M_{\rm BH}/M_\star$ (the BH–stellar mass ratio), respectively.

star-forming gas, and higher ages. Such systems also tend to be dispersion-supported, on average (Figs 1 and 3). A preliminary analysis of the merger histories of EAGLE galaxies suggests that massive galaxies with lower O/H seem to have been subjected to major mergers events, which inhibited the formation of a disc and also contributed to the increase of the central BH mass. The analysis of the formation histories of EAGLE galaxies and its connection to the scatter of the MZR will be the subject of a forthcoming article (Zenocratti et al., in preparation).

Sharma & Theuns (2019) propose a model of self-regulated galaxy formation, in which the SFR, stellar mass, gas mass, and metallicity depend on halo mass, cosmological accretion rate, and redshift, but regulated by feedback. In their 'I$\kappa\epsilon\alpha$' model, the main astrophysical parameter ϵ is a dimensionless measure of the efficiency of stellar feedback: a large value of ϵ implies efficient feedback and low SFR, while feedback is inefficient and the SFR is high for a small ϵ. This leads to the following scaling for Z and $f_{\rm g}$ with $M_\star$ and efficiency ϵ:

$$Z \propto \frac{M_\star^{2/5}}{\epsilon^{3/5}}\,; \quad f_{\rm g} \propto \frac{\epsilon^{\frac{2}{5}\frac{n-1}{n}}}{M_\star^{\frac{3}{5}\frac{n-1}{n}}} \approx \frac{\epsilon^{0.11}}{M_\star^{0.17}}\,, \tag{1}$$

where $n \approx 1.4$ is the slope of the Kennicutt–Schmidt star formation law. These relations show that when feedback is efficient (meaning ϵ is large, $\epsilon \approx 1$), Z is low and $f_{\rm g}$ is high, whereas, inefficient feedback ($\epsilon \ll 1$) implies Z is high and $f_{\rm g}$ low. We can connect this to the morphology of the galaxy by speculating that feedback in a thin disc – corresponding to a galaxy with high $\kappa_{\rm co}$ – is more efficient than when $\kappa_{\rm co}$ is low (a more spheroidal gas distribution). High-resolution simulations that resolve individual supernova energy injections in gas columns suggest this type of relation between feedback efficiency and disc morphology. For example, the simulations by Creasey, Theuns & Bower (2013) show that supernova explosions that occur above or below the disc are more efficient at driving winds, because cooling loses are suppressed when the explosion occurs at the lower densities that prevail there (see also Girichidis et al. 2016). Thus, in EAGLE, accretion of metal-poor gas seems to trigger the formation of a disc but, once the disc has already been formed, feedback effects would play a role in regulating the subsequent metallicity evolution. We leave the analysis of feedback effects on EAGLE disky galaxies for a future work.

5 CONCLUSIONS

We analysed the MZR as a function of morpho-kinematical parameters in the EAGLE cosmological hydrodynamical simulations. At $z = 0$, we found new secondary dependences of metallicity on the internal kinematics and morphology of galaxies. At low masses ($M_\star \lesssim 10^{10}$ M$_\odot$), higher metallicities are found for more spheroidal and lower rotation-supported galaxies.

A preliminary analysis of the star formation histories of low-mass galaxies indicates that late accretion of metal-poor gas dilutes the metal content of galaxies, triggers their star formation activity, and contributes to the formation of the galaxy disc. When the gas is in a thin, rotationally supported disc, feedback may be more efficient, which results in lower O/H and a higher gas fraction (Sharma & Theuns 2019). The trends in more massive galaxies are generally less strong, with lower metallicities found in more prolate galaxies with lower levels of rotational support. AGN feedback and mergers seem to play a key role in shaping the MZR at the

high-mass end. At increasing redshifts, the trend between rotational support and metallicity becomes weaker at low stellar mass but more pronounced at high stellar mass. These trends are consistent with the secondary dependences of O/H (at a fixed mass) on gas fraction, SFR, and stellar age, and the relation between the latter quantities with galaxy morpho-kinematics (see DR17).

Our findings regarding the O/H secondary dependences (at fixed stellar mass) on morpho-kinematics and their relation with the scatter of the MZR were not previously discussed in the literature. A detailed analysis of the origin and evolution of the mass–metallicity–morpho-kinematics relation in EAGLE will be presented in a future article.

ACKNOWLEDGEMENTS

LJZ and MEDR acknowledge support from PICT-2015-3125 of Agencia Nacional de Promoción Científica y Tecnológica, PIP 112-201501-00447 of Consejo Nacional de Investigaciones Científicas y Técnicas and UNLP G151 of Universidad Nacional de La Plata (Argentina). MALL is a DARK-Carlsberg Foundation Fellow (Semper Ardens project CF15-0384). We acknowledge the Virgo Consortium for making their simulation data available. The EAGLE simulations were performed using the DiRAC-2 facility at Durham, managed by the ICC, and the PRACE facility Curie based in France at TGCC, CEA, Bruyères-le-Châtel. This work used the DiRAC@Durham facility managed by the Institute for Computational Cosmology on behalf of the STFC DiRAC HPC Facility (www.dirac.ac.uk). The equipment was funded by BEIS capital funding via STFC capital grants ST/P002293/1, ST/R002371/1, and ST/S002502/1, Durham University, and STFC operations grant ST/R000832/1. DiRAC is part of the National e-Infrastructure.

REFERENCES

Bothwell M. S., Maiolino R., Kennicutt R., Cresci G., Mannucci F., Marconi A., Cicone C., 2013, MNRAS, 433, 1425
Calura F., Pipino A., Chiappini C., Matteucci F., Maiolino R., 2009, A&A, 504, 373
Calvi R., Vulcani B., Poggianti B. M., Moretti A., Fritz J., Fasano G., 2018, MNRAS, 481, 3456
Camps P. et al., 2018, ApJS, 234, 20
Correa C. A. et al., 2017, MNRAS, 472, L45
Crain R. A. et al., 2015, MNRAS, 450, 1937
Creasey P., Theuns T., Bower R. G., 2013, MNRAS, 429, 1922
Davé R., Anglés-Alcázar D., Narayanan D., Li Q., Rafieferantsoa M. H., Appleby S., 2019, MNRAS, 486, 2827
De Rossi M. E., Theuns T., Font A. S., McCarthy I. G., 2015, MNRAS, 452, 486
De Rossi M. E., Bower R. G., Font A. S., Schaye J., Theuns T., 2017, MNRAS, 472, 3354
Ellison S. L., Patton D. R., Simard L., McConnachie A. W., 2008, ApJ, 672, L107
Furlong M. et al., 2015, MNRAS, 450, 4486
Furlong M. et al., 2017, MNRAS, 465, 722
Girichidis P. et al., 2016, MNRAS, 456, 3432
Lara-López M. A. et al., 2010, A&A, 521, L53
Lara-López M. A. et al., 2013, MNRAS, 433, L35
Lara-López M. A., De Rossi M. E., Pilyugin L. S., Gallazzi A., Hughes T. M., Zinchenko I. A., 2019, MNRAS, 490, 868
Ma X. et al., 2016, MNRAS, 456, 2140
McAlpine S. et al., 2016, Astron. Comput., 15, 72
Mannucci F., Cresci G., Maiolino R., Marconi A., Gnerucci A., 2010, MNRAS, 408, 2115
Planck Collaboration XXIII, 2015, A&A, 580, A13
Sánchez S. F. et al., 2019, MNRAS, 484, 3042
Sánchez Almeida J., Dalla Vecchia C., 2018, ApJ, 859, 109
Schaye J. et al., 2015, MNRAS, 446, 521
Sharma M., Theuns T., 2019, MNRAS, preprint (arXiv:1906.10135)
Springel V., 2005, MNRAS, 364, 1105
Telford O. G., Dalcanton J. J., Skillman E. D., Conroy C., 2016, ApJ, 827, 35
The EAGLE Team, 2017, preprint (arXiv:1706.09899)
Thob A. C. R. et al., 2019, MNRAS, 485, 972
Torrey P. et al., 2018, MNRAS, 477, L16
Torrey P. et al., 2019, MNRAS, 484, 5587
Trayford J. W. et al., 2015, MNRAS, 452, 2879
Trayford J. W., Frenk C. S., Theuns T., Schaye J., Correa C., 2019, MNRAS, 483, 744
Tremonti C. A. et al., 2004, ApJ, 613, 898
Troncoso P. et al., 2014, A&A, 563, A58
Wu Y.-Z., Zhang W., Zhao Y.-H., 2019, MNRAS, 486, 5310
Yates R. M., Kauffmann G., Guo Q., 2012, MNRAS, 422, 215

This paper has been typeset from a TEX/LATEX file prepared by the author.